REPORT DOCUMENTATION PAGE

2

Form Approved OMB NO. 0704-0188

1. REPORT DATE (DD-MM-YYYY)	2. REPORT TYPE	3. DATES COVERED (From - To)
	New Reprint	-

4. TITLE AND SUBTITLE

Chiral Plasmonic Nanostructures on Achiral Nanopillars

5a. CONTRACT NUMBER
W911NF-12-1-0407

5b. GRANT NUMBER

5c. PROGRAM ELEMENT NUMBER
611103

6. AUTHORS

Bongjun Yeom,† Huanan Zhang,† Hui Zhang,‡ Jai Il Park,†,§ Kyoungwon Kim,† Alexander O. Govorov,*,‡, and Nicholas A. Kotov*,†

5d. PROJECT NUMBER

5e. TASK NUMBER

5f. WORK UNIT NUMBER

7. PERFORMING ORGANIZATION NAMES AND ADDRESSES

William Marsh Rice University
6100 Main St., MS-16

Houston, TX 77005 -1827

8. PERFORMING ORGANIZATION REPORT NUMBER

9. SPONSORING/MONITORING AGENCY NAME(S) AND ADDRESS (ES)

U.S. Army Research Office
P.O. Box 12211
Research Triangle Park, NC 27709-2211

10. SPONSOR/MONITOR'S ACRONYM(S)
ARO

11. SPONSOR/MONITOR'S REPORT NUMBER(S)
61796-CH-MUR.30

12. DISTRIBUTION AVAILIBILITY STATEMENT

Approved for public release; distribution is unlimited.

13. SUPPLEMENTARY NOTES

The views, opinions and/or findings contained in this report are those of the author(s) and should not contrued as an official Department of the Army position, policy or decision, unless so designated by other documentation.

14. ABSTRACT

Chirality of plasmonic films can be strongly enhanced by threedimensional (3D) out-of-plane geometries. The complexity of lithographic methods currently used to produce such structures and other methods utilizing chiral templates impose limitations on spectral windows of chiroptical effects, the size of substrates, and hence, further research on chiral plasmonics. Here we demonstrate 3D chiral plasmonic nanostructures (CPNs) with high

15. SUBJECT TERMS

Chirality, plasmonic chirality, ZnO, nanopillars, circular dichroism, three-dimensional thin films, 3D chirality

16. SECURITY CLASSIFICATION OF:			17. LIMITATION OF ABSTRACT	15. NUMBER OF PAGES	19a. NAME OF RESPONSIBLE PERSON
a. REPORT	b. ABSTRACT	c. THIS PAGE			Naomi Halas
UU	UU	UU	UU		19b. TELEPHONE NUMBER 713-348-5746

Report Title

Chiral Plasmonic Nanostructures on Achiral Nanopillars

ABSTRACT

Chirality of plasmonic films can be strongly enhanced by threedimensional (3D) out-of-plane geometries. The complexity of lithographic methods currently used to produce such structures and other methods utilizing chiral templates impose limitations on spectral windows of chiroptical effects, the size of substrates, and hence, further research on chiral plasmonics. Here we demonstrate 3D chiral plasmonic nanostructures (CPNs) with high optical activity in the visible spectral range based on initially achiral nanopillars from ZnO. We made asymmetric gold nanoshells on the nanopillars by vacuum evaporation at different inclination and rotation angles to achieve controlled symmetry breaking and obtained both left- and rightrotating isomers. The attribution of chiral optical effects to monolithic enantiomers made in this process was confirmed by theoretical calculations based on their geometry established from scanning electron microscope (SEM) images. The chirality of the nanoshells is retained upon the release from the substrate into a stable dispersion. Deviation of the incident angle of light from normal results in increase of polarization rotation and chiral g-factor as high as ?0.3. This general approach for preparation of abiological nanoscale chiral materials can be extended to other out-of plane 3D nanostructures. The large area films made on achiral nanopillars are convenient for sensors, optical devices, and catalysis.

REPORT DOCUMENTATION PAGE (SF298)
(Continuation Sheet)

Continuation for Block 13

ARO Report Number 61796.30-CH-MUR
Chiral Plasmonic Nanostructures on Achiral Nar...

Block 13: Supplementary Note

Approved for public release; distribution is unlimited.

NANO LETTERS

Letter

pubs.acs.org/NanoLett

Chiral Plasmonic Nanostructures on Achiral Nanopillars

Bongjun Yeom,[†] Huanan Zhang,[†] Hui Zhang,[‡] Jai Il Park,[†,§] Kyoungwon Kim,[†] Alexander O. Govorov,*[,‡] and Nicholas A. Kotov*[,†]

[†]Departments of Chemical Engineering, University of Michigan, Ann Arbor, Michigan 48109, United States

[‡]Department of Physics, Ohio University, Athens, Ohio 45701, United States

Supporting Information

ABSTRACT: Chirality of plasmonic films can be strongly enhanced by three-dimensional (3D) out-of-plane geometries. The complexity of lithographic methods currently used to produce such structures and other methods utilizing chiral templates impose limitations on spectral windows of chiroptical effects, the size of substrates, and hence, further research on chiral plasmonics. Here we demonstrate 3D chiral plasmonic nanostructures (CPNs) with high optical activity in the visible spectral range based on initially achiral nanopillars from ZnO. We made asymmetric gold nanoshells on the nanopillars by vacuum evaporation at different inclination and rotation angles to achieve controlled symmetry breaking and obtained both left- and right-rotating isomers. The attribution of chiral optical effects to monolithic enantiomers made in this process was confirmed by theoretical calculations based on their geometry established from scanning electron microscope (SEM) images. The chirality of the nanoshells is retained upon the release from the substrate into a stable dispersion. Deviation of the incident angle of light from normal results in increase of polarization rotation and chiral *g*-factor as high as −0.3. This general approach for preparation of abiological nanoscale chiral materials can be extended to other out-of plane 3D nanostructures. The large area films made on achiral nanopillars are convenient for sensors, optical devices, and catalysis.

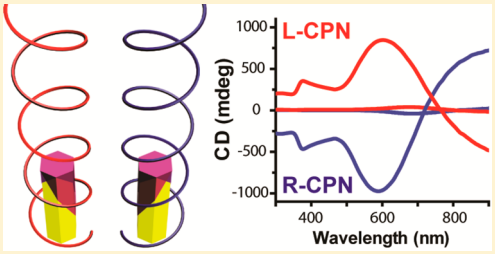

KEYWORDS: *Chirality, plasmonic chirality, ZnO, nanopillars, circular dichroism, three-dimensional thin films, 3D chirality*

Since helical organizational motifs were discovered in proteins and DNA, much attention has been paid to optically active materials which have so-called "handedness" or chirality.[1,2] In addition to elucidation of their chirality-dependent functions in living systems, which typically display levorotating chirality, there have been large efforts to develop man-made chiroptical materials with controlled right- (R-) and left- (L-) handedness for applications as negative refractive index media,[3,4] biosensors,[5] enantioselective separation, and catalysis.[1] One of the central targets for materials design in this area is the increase of the anisotropy factor *g* exceeding those for natural biomolecules[6] by 2−3 orders of magnitude, especially in the visible part of electromagnetic spectrum. Chiral materials based on individual nanoparticles (NPs)[7,8] or their assemblies[9,10] have attracted much attention because of the tunability of their absorption bands. Plasmonic systems are particularly promising in this respect because the extinction of plasmons that can yield chiral structures with exceptionally high *g* values, materials referred to as "superchiral".[5,11−13]

Besides the synthesis of NPs with chiral inorganic cores,[8,14,15] there have been three predominant basic approaches to the fabrication of chiral plasmonic nanostructures (CPNs). (1) Most often CPNs are made on chiral templates by spontaneous attachment of gold or silver NPs to chiral (bio)polymers displaying helical or similar configurations.[11,16−19] (2) Another method that is used less frequently for making CPNs is the "tinker-toy" approach. This is based on the ability of biological molecules, such as DNA, to hybridize into geometrically controlled assemblies. This method was used as a tool to produce three-dimensional (3D) NP assemblies with different chiral geometries: tetrahedral,[9,10,20] helical, and cross-rod patterns[21,22] were demonstrated. (3) Latest developments in lithography and were applied to produce 2D or 3D nanoscale sculpted gold coatings.[5,13,23,24] Arrays of Au nanodots or other Au nanoscale patterns were made by applying several rounds of electron beam lithography.[5,23] In another representation, microsize helical structures were made by 3D direct laser writing,[24] demonstrating broad-range chiroptical activity in the IR and far IR range. In addition, recent progress has been made to reduce feature size of plasmonic structures down to nanometer scale via control of directional deposition of noble metals.[25−27] These concurrent techniques have brought chiroptical window shifted in visible range. The great advantages of lithography for CPNs include the ability to produce defined 3D geometries and the availability of commercial lithography systems.

Although great progress has been made in the synthesis of CPNs, there are still significant limitations inherent in each of these techniques. The complexity of the synthesis of polymeric templates is one of them. The self-assembly process used, for

Received: July 26, 2013
Revised: October 7, 2013
Published: October 10, 2013

   dx.doi.org/10.1021/nl402782d | *Nano Lett.* 2013, 13, 5277−5283

instance in our previous work,[28] requires delicate modification of NPs.[9,10,20] Scaling up of pure enantiomer synthesis of tetrahedral NP assemblies is challenging as well. The process of repetitive e-beam lithography, including resist deposition, mask alignment, e-beam exposure, resist removal, and so forth, is tedious and expensive. Although highly accurate, this technique is limiting with respect to the total patterned area of a sample. It takes about one week to pattern a 30 mm diameter wafer on one side. Direct-write 3D laser lithography is capable of making 3D CPNs. Unfortunately, it currently lacks sufficient resolution to make 3D features less than 100 nm[29,30] that would be desirable for polarization rotation in the visible range. These size limitations restrict the current applicability of 3D lithography to the IR range. Other methods based on glancing angle deposition[31,32] also have the limitations related to both size of the features and the limited availability of equipment.[25−27] It would be desirable to make CPNs with 100 nm scale that could be useful for sensors, nanoscale optical devices, and catalysis and would have strong chiroptical activity substantially exceeding that observed for single metallic NPs that have dimensions of few nanometers in diameter.

Here we present a method to prepare CPNs with 3D geometry and strong chiral optical activity in the visible light range without the use of chiral templates, complex synthetic protocols, or multistep lithography. The method is simple and applicable to substrates of a variety of sizes without increase in processing time. Out-of-plane 3D geometry of CPNs greatly increases coupling with light photons with normal incidence. To obtain such geometry we initially grow ZnO nanopillars onto quartz or glass substrates via hydrothermal synthesis[33] (Figure 1a). The first Au layer is then deposited on the ZnO nanopillars. Note that the substrate is inclined in respect to the direction of the flux of Au atoms in order to have one-sided deposition (Figure 1b). The asymmetric deposition of a ca. 5 nm thick gold layer occurs over the entire sample at the same time. After cutting the sample in half (Figure 1c), each piece was subjected to the deposition of a second layer of gold. The substrate is now inclined at a different angle and rotated in order to create nanoshells with geometries that are non-superimposable in space (symmetry breaking). The first and the second halves of the sample were rotated in opposite directions before applying the second Au layer with a thickness of ca. 10 nm. In other words, one piece was placed under the beam of Au atoms coming from the direction described by an angle of $\alpha = +90°$ (L-CPN, left of Figure 1d), and another piece was placed such that the flux comes from $\alpha = -90°$ (R-CPN, right of Figure 1d). The fact that this process produces arrays of nanopillars which have mirror geometries can be seen in Figure 1e. L-CPNs and R-CPN were obtained by rotating the substrate in the counterclockwise and clockwise directions, respectively.

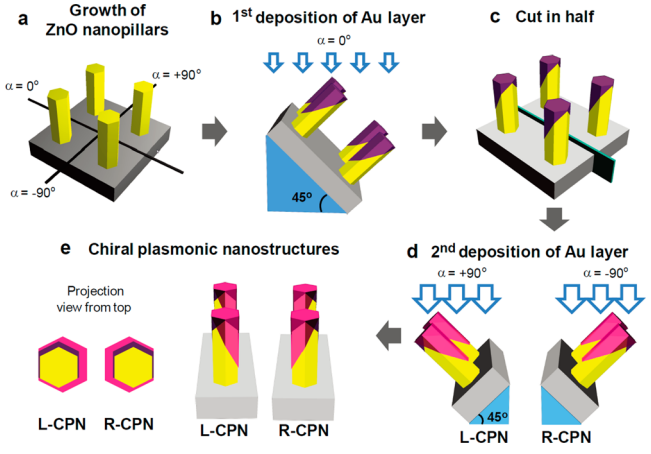

Figure 1. Schematics of the fabrication process. (a) ZnO nanopillars are grown onto substrate. (b) The first Au layer is deposited on top of ZnO nanopillar arrays from direction of $\alpha = 0°$ with an inclined angle of 45°. (c) Samples are cut in half. (d) The second Au layer is deposited on each sample with different rotation. For the L-CPN sample, the direction of Au deposition is rotated to be incident from the direction of $\alpha = +90°$. The other sample, R-CPN, is aligned to be exposed from $\alpha = -90°$ direction. (e) Asymmetric deposition of Au layers with inclined angle provides chiral nanostructures of Au-shell-coated ZnO nanopillars. A tilted view from $\alpha = 180°$ and the projection view from top are presented with schematics.

Individual ZnO nanopillars coated with Au nanoshells in L-CPN and R-CPN configurations prepared as above were imaged by scanning electron microscopy (SEM) from different sides (Figure 2, Au layer is artificially colored to enhance the contrast). The images of L-CPN taken from $\alpha = 0°$ and +90° show distinct Au layers onto ZnO nanopillars since these sides are exposed to the gold deposition (Figure 2a). On the other hand the views from −90° and 180° for L-CPN show that only half of the ZnO nanopillars are covered with Au since most of incident gold atoms are screened by the shadowing effect. In the case of R-CPN, almost same images were obtained to those for L-CPN, but in mirror-reflected view directions (Figure 2b). For instance, R-CPN image from +90° represents same shape of Au nanoshell comparing to L-CPN image from −90°.

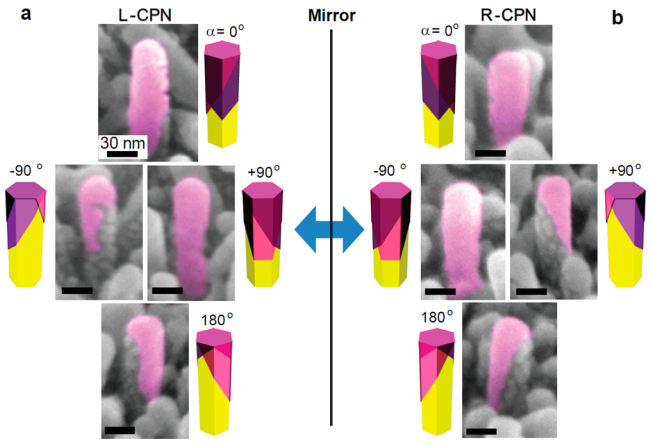

Figure 2. Tilted SEM images of CPNs. Tilted SEM images of (a) L-CPN and (b) R-CPN viewed from different angles. The relative direction of the views is given in the corner of each image. Au layers are artificially colored to improve contrast. The original images are given in Supporting Information. Scale bars represent 30 nm.

The optical activity of CPNs was examined by circular dichroism (CD) spectroscopy (Figure 3). CD spectra obtained for different aspect ratios (r) of ZnO nanopillars clearly demonstrate that it is possible to manipulate chiroptical activity of the pillar-based CPNs in terms of spectral position and amplitude of the plasmonic band. Importantly, the optical effects of linear birefringence (LB) and linear dichroism (LD) are minor as indicated by a series of dedicated tests including the "front-and-back" and "rotation" CD measurements of the samples (Supporting Information S7 and S8). The direction of the incident light was parallel to the long axis of ZnO

dx.doi.org/10.1021/nl402782d | Nano Lett. 2013, 13, 5277−5283

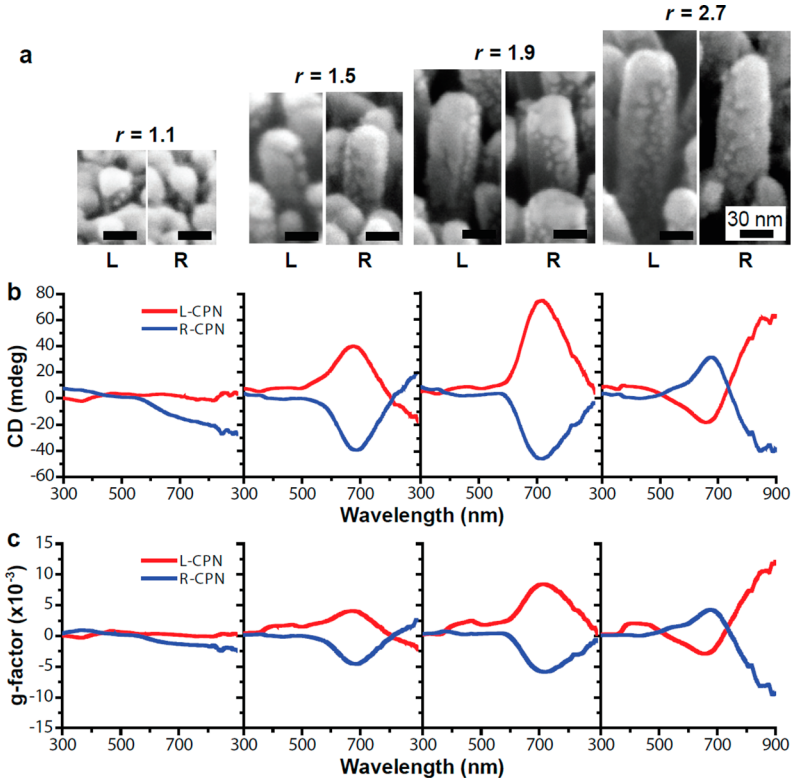

Figure 3. Optical activity of CPNs with different aspect ratios. (a) Tilted SEM images show various aspect ratios of Au nanoshells on ZnO nanopillars. (b) Circular dichroism and (c) *g*-factor of L-CPN and R-CPN are plotted with increasing order of aspect ratios from left to right. In all cases, the L- and R-CPN CD spectra are mirrored with respect to each other. All of the spectra were taken for the normal incidence of light to the substrates and UV−vis absorbance spectra are given in the SI.

nanopillars; the incoming photons had normal incidence with respect to the substrate. Having said that, we also need to note that LB and LD effects are potentially possible in nanopillar arrays; however for our samples that have randomized orientation of ZnO and Au crystal lattices and inclinations of the nanopillars, such effects are likely to be observed only in sub-500 nm scale for spatially localized CD optical measurements.

When the aspect ratio of CPNs (r) was small, for example, r = 1.1, no peaks were observed in the CD spectra for either L-CPN or R-CPN. ZnO nanopillars of this size display negligible difference in geometry between L-CPN and R-CPN. The lack of 3D features protruding in the normal direction to the substrate results in a nearly continuous Au film approaching the morphology of the flat surface as indicated in broadening of surface plasmonic absorption peak (see Supporting Information S5).

When the r value of the CPNs was increased to 1.5, the obtained CD spectra showed distinct chirality. The peaks of the CD spectra obtained for L-CPN and R-CPN were opposite in sign; they mirrored each other with respect to the wavelength axis (Figure 3b). L-CPN displayed positive rotation in the visible range with a maximum located at 680 nm and amplitude of +40 mdeg. Concurrently, the R-CPN sample displayed negative rotation with a maximum at the same wavelength and an amplitude of −39 mdeg.

When r was further increased to 1.9, the amplitude of CD spectra increased to +74 mdeg and to −47 mdeg for L-CPN and R-CPN, respectively. The increase of length of ZnO nanopillars, and therefore also the Au nanoshells, resulted in the shift of spectral position of the maximum peak to 715 nm. For r = 2.7, the maximum amplitude peaks of both CPNs red-shifted toward 900 nm, which is the limit of the detector available for this study. The amplitudes of the peaks were similar to those of CPNs with r = 1.9. One could also notice in Figure 3 that an increase of the aspect ratio to r = 2.7 results in the appearance of an additional weaker peak at 660 and 675 nm for L-CPN and R-CPN, respectively. We attribute the appearance of this peak to the Coulombic interaction[34] of plasmons in the adjacent nanopillars. Their deviation from the perfectly mutually parallel orientation becomes stronger for r = 2.7, resulting in hybridization[16,21,35] and splitting of the plasmon band, and allows more antiparallel plasmon oscillations in adjacent pillars. Similar observations on oppositely polarized bands in CD spectra have been reported in the other plasmonic systems.[11,16,20,36] Plasmonic modes in a nanocrystal with a chiral surface distortion should also be taken into account.[37]

The chiral anisotropy factor, also known as the *g*-factor, is defined as $\Delta\varepsilon/\varepsilon$, where $\Delta\varepsilon$ and ε are the molar circular dichroism and molar extinction, respectively. When the aspect ratio of ZnO nanopillars was increased from r = 1.5 to 2.7, the maximum *g*-factors increased from +0.004 to +0.012 for L-CPN and from −0.005 to −0.010 for R-CPN (Figure 3c). For higher aspect ratios of anisotropic CPNs, the longitudinal mode of surface plasmon dominates over the transverse mode, which could be expected given a better coupling of incident light with protruding 3D features, and thereby stronger optical rotation.[21,38,39]

The chiral Au nanoshells have the ability to impart chiroptical activity to achiral ZnO nanopillars, as indicated by the appearance of CD peaks at 375 nm corresponding to

dx.doi.org/10.1021/nl402782d | *Nano Lett.* 2013, 13, 5277−5283

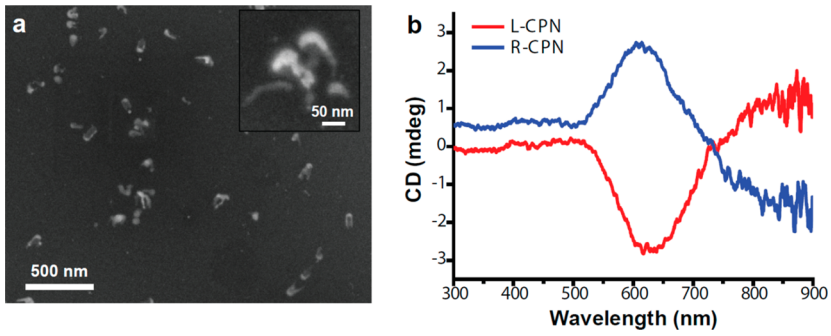

Figure 4. Au nanoshells released into water. (a) SEM image of L-CPN nanoshells. The higher magnification image is shown in inset. (b) Circular dichroism of the released L-CPN and R-CPN in dispersions.

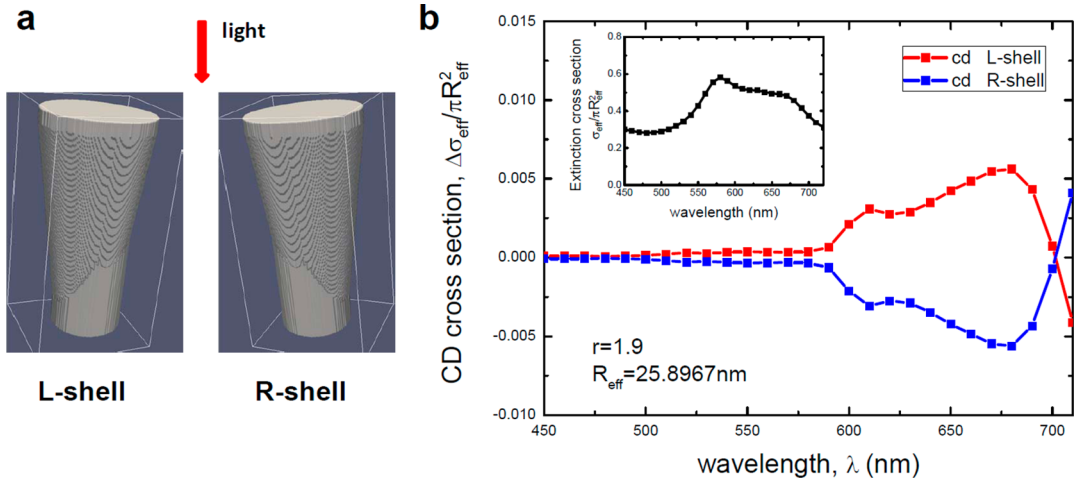

Figure 5. Computational simulation of the optical behavior of CPNs. (a) Models of the chiral nanoshells. (b) Calculated CD cross section for the L- and R-nanoshells. Inset: Extinction of the nanoshells for the normal incidence of light.

optical extinction of ZnO nanopillars (Figure 3b). ZnO nanopillars and NPs grown by hydrothermal methods do not display any optical activity on their own (Supporting Information). However, when the chiral Au nanoshells cover the achiral ZnO nanopillars, the asymmetric electrostatic field generated by chiral plasmons in Au nanoshells couples with oscillation of charge carriers in the ZnO nanopillars and hence generates chiral absorption of the achiral ZnO nanopillars. Similar phenomena have been observed for achiral nanoparticles when chiral organic molecules are adsorbed on the surface of them.[40,41] A difference in the origin of the induced chirality here is that the dissymmetric field originates from "designed" chiral Au nanoshells rather than from a natural amino acid or other components.

To confirm our attribution of chiroptical phenomena discussed above, we decided to verify that the Au nanoshells have chiral geometries by themselves when they are separated from the nanopillars. Au nanoshells were carefully released from the r = 1.9 ZnO nanopillars and transferred into aqueous dispersions. Initially, water-dispersible surfactant, PEG-SH, was attached to the surface of the Au nanoshells by dipping the substrates into 0.1 wt % PEG-SH aqueous solution for 1 h at room temperature. Then ZnO was dissolved in water (pH 2) with 10 s of ultrasonication. The nanoshells formed stable dispersions with absorption spectra typical for anisotropic Au nanoparticles, having a transverse mode peak at 550 nm and a longitudinal mode peak at 890 nm (Supporting Information). The shape of the released Au nanoshells is clearly retained after dissolving the ZnO nanopillars (Figure 4a). The chiroptical activity of the Au nanoshells was preserved in these dispersions: the CD spectra of the dispersions of previously deposited Au nanoshells demonstrated mirror symmetry of the CD spectra and bisignate shape (Figure 4b) typical for the plasmonic CD mechanism of chiral objects.[34] The blue shift of the CD spectra in solution compared to the same shells on the substrate is associated with the screening effect of the dielectric substrate and neighboring nanopillars on a substrate. CD spectra of our Au nanoshells on a substrate and in solution are inverted (Figures 3b and 4b). This is not so surprising since the CD signals in solution are averaged over all directions, whereas the CD on substrate corresponds to one (normal) direction. Strong directional CD signals calculated for various angles of incidence often flip as we change the direction of incidence,[42] as it is the case for our system. Also, a magnitude of an averaged CD (i.e., CD in solution) usually is smaller than that of CD signals of oriented chiral species.[42] Therefore, the signs of directional and solution CD spectra can be flipped and are not strictly correlated in sign, but both, of course, appear at the plasmon resonance band. Such behavior was recently demonstrated numerically for chiral plasmonic superstructures of various geometries (see Figure 7 in ref 42). Other differences between the two systems (in solution and on substrate), which can modify the CD spectrum, are the dielectric ZnO core and the dielectric substrate; the plasmonic CD effect is sensitive to the dielectric environment. The maximum g-factors in dispersed CPNs are −0.0012 for L-CPN and +0.0011 for R-CPN

dx.doi.org/10.1021/nl402782d | *Nano Lett.* 2013, 13, 5277−5283

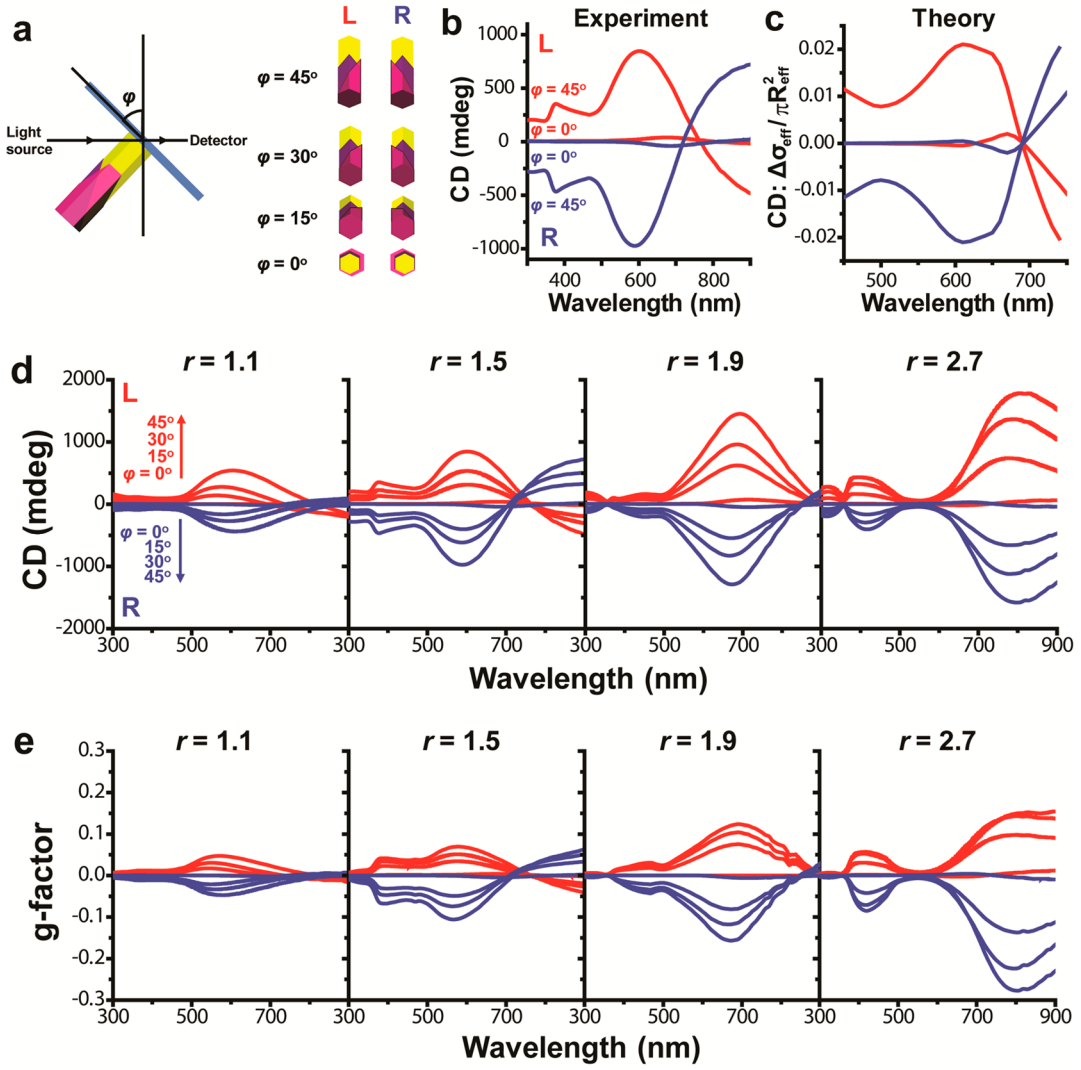

Figure 6. (a) Configuration of tilting angle (φ) of CPNs related to the incident circularly polarized light and projection views of CPNs from the beam source. (b) Experimental CD spectra and (c) theoretical results of L-CPN and R-CPN (r = 1.5) with normal incidence (φ = 0°) and inclined incidence (φ = 45°) (d) CD spectra and (e) g-factors measured from different aspect ratios of CPNs are shown in order of r = 1.1, 1.5, 1.9, and 2.7 from left to right with change of tilting angle (φ).

(Supporting Information), which are 1 order of magnitude smaller than the g-factor observed when ZnO nanopillars are present. This reduction is expected due to random orientation of the CPNs in solution and confirms the importance of the 3D out-of-plane character of ZnO nanopillar substrates allowing the efficient coupling with incoming photons. Compared to the templation of NPs on biomacromolecules and self-assembly techniques[9,11,20] or similar methods based on biomacromolecules,[43] the shape of chiral monolithic NPs with controlled handedness is atypical and does not replicate the tetrahedral or helical patterns used previously.

To confirm the attribution of chiroptical activity to the complex chiral shape of the Au caps on ZnO nanopillars, we decided to computationally simulate optical responses of CPNs at the normal incidence of light using the discrete dipole approximation (DDA) code developed recently (Supporting Information). The geometrical models used in the calculations were two Au-shells partially covering a cylinder with r = 1.9 (Figure 5a). For simplicity and faster convergence of DDA, we removed the ZnO substrate and considered isolated nanostructures in air (see Methods).

First we calculated the extinction spectrum of the nanostructure (inset in Figure 5b) that could be compared to the UV−vis absorption spectrum. The model CPNs displayed a theoretical plasmon peak at 580 nm. It was blue-shifted compared to the experimentally observed spectrum, which indicated that the plasmons in actual Au nanoshells were electrostatically coupled to each other in the nanopillar arrays (Supporting Information) as discussed above. The ZnO nanopillars should create additional dielectric screening for plasmons and therefore shift the plasmon bands to the red. The calculated CD spectra at the normal incidence (Figure 5) qualitatively reproduce the experimental data (Figure 3 for r = 1.5−1.9). The calculated CD spectrum displayed a plasmonic band at 600−700 nm with an expected slight blue-shift compared to the experimental spectra. The change in the chirality of the nanoshells leads to a flip of the CD signal (Figure 5). Because of the chiral shape of nanoshells, optically induced plasmonic currents and plasmon oscillations in the nanoshells also become chiral.[37] Note that this mechanism is different from the dipolar plasmonic CD in assemblies of

dx.doi.org/10.1021/nl402782d | Nano Lett. 2013, 13, 5277−5283

spherical nanoparticles where the particle−particle plasmonic interactions create CD and chiral plasmonic excitations.[11,20,34]

Since CPNs are vertically aligned to the substrates and highly anisotropic, one could expect their orientation with respect to the incident light to affect CD responses.[44,45] Optical activities of CPNs were investigated, while substrates were tilted to an angle of φ as presented in Figure 6a. A change of tilting angle from 0° to 45° strongly enhances CD signals of both L-CPN and R-CPN (Figure 6b). These results match theoretical calculation obtained by DDA for the same light incidence conditions (Figure 6c). The amplitude of CD band for L-CPN increased from +40 mdeg to +847 mdeg—that is 20 times—as φ changed from 0° to 45°. For R-CPN, it increased from −39 mdeg to −974 mdeg, or by 25 times, for the same tilt angles. The position of peaks is shifted to lower wavelengths compared to normal incidence light. The enhancement of CD signal is more pronounced when the aspect ratio of chiral plasmonic nanostructure is increased (Figure 6d).

The strongest optical activity is observed in the highest aspect ratio of 2.7. At tilting angle of 45°, the maximum amplitude is reaching to +1780 mdeg for L-CPN and −1580 mdeg for R-CPN. In addition, *g*-factor of corresponding CPN pairs reaches up to +0.15 for R-CPN and −0.28 for L-CPN. The amplitude of the *g*-factor of the CPNs in this work is comparable to the strongest surface plasmonic optical activity in the visible range observed in recent studies.[11,25,27] It should be noted that the typical order of magnitude of *g*-factors of surface CPNs is below 10^{-3} in most cases.[11,16]

Abiological 3D CPNs were prepared by sequential deposition of two Au layers on achiral nanopillars. Symmetry breaking between left- and right-rotating enantiomers was achieved by changing the deposition angles between first and second gold layers. Optical activity of these 3D CPNs can be tuned from 550 to 900 nm by adjusting only the aspect ratio of the nanopillars. The unidirectional orientation of chiral plasmonic elements increases the *g*-factor compared to dispersions where their orientation is random by 10 times. Tilting of the samples in respect to the laser beam gives further increase of the *g*-factor that matches theoretical expectations. This pathway for the preparation of chiral coatings can be universally applied to a diverse range of corrugated nanopatterns (for examples, silica nanoparticles, see SI Figure S4) and materials. A high *g*-factor, combined with simplicity of the preparation of the chiral plasmonic coatings, and its lithography-less nature make this technique convenient for practical application exemplified by the development of negative refractive index material for perfect lens,[3] ultrasensitive biosensor using a chiral field,[5] and ultrathin polarized coating in the visible range.

Methods. *Fabrication of ZnO Nanopillars.* ZnO nanoparticles were synthesized as described elsewhere with ultrasonication to avoid aggregation of nanoparticles (references in Supporting Information). As-prepared ZnO nanoparticles were deposited onto substrates by immersion for 10 min, followed by rinsing with methanol and drying with a gentle stream of air. ZnO nanopillars were grown onto ZnO nanoparticle-deposited substrates via hydrothermal reaction with equimolecular amounts of zinc nitrate hexahydrate (Sigma-Aldrich, >99%) and hexamethylenetetramine (Sigma-Aldrich, >99%) aqueous solutions at 90 °C for a range of reaction times. Typically, growth times of 30, 60, 90, and 120 min were used for aspect ratios of r = 1.1, 1.5, 1.9, and 2.7, respectively.

Asymmetric Deposition of Au Layers. An e-beam evaporator was used to deposit Au layers on ZnO NWs. First, an Au layer was deposited with 5 nm thickness, and a second layer was deposited with 10 nm thickness. Substrates with ZnO nanopillars were placed in a chamber with a sample holder with an inclined angle of 45°. The back side of the substrate was washed off to remove residue of ZnO or Au.

Release of Au Nanoshells. Au nanoshells with ZnO nanopillars on substrate were immersed in 0.1 wt % of PEG-SH (polyethylene glycol with thiol groups, Laysan Bio Inc. M_w = 5k) aqueous solution for 1 h, followed by rinsing with DI water to remove unbound PEG-SH. Then, substrate was immersed in pH ∼ 2 acidic solution with 10 s of ultrasonication to dissolve ZnO nanopillars.

Characterization. SEM images were obtained with a FEI Nova system. CD and UV−vis spectra were obtained with a Jasco J-815 CD spectrometer and Agilent 8453 UV−vis spectrometer, respectively.

Modeling. The results given here are based on a numerical solution of Maxwell's equations incorporating local dielectric functions of gold and ZnO. The ZnO-cylinder and Au shells have dielectric functions ε_{ZnO} = 3.8 and $\varepsilon_{Au}(\omega)$, where the function $\varepsilon_{Au}(\omega)$ is taken from a reference in the Supporting Information. The matrix is air (ε_{matrix} = 1). As a numerical method, we employed the discrete dipole approximation (DDA) and software from references in the Supporting Information.

A model of a chiral nanocrystal (Figure 5a) is composed of a ZnO-cylinder (along the *z*-direction) and two Au shells made in the *x*- and *y*-directions. This geometry is chiral. The dimensions of the components of the nanostructure are chosen to mimic the experimental structures with r = 1.9 (Figure 3). The sizes used in the modeling are the following: the radius of the ZnO cylinder was 14 nm, cylinder length of 80 nm, lengths of the first and second Au-shells 50 and 74.8 nm, radii of the first and second Au-shells 17 and 19.25 nm, and the thickness of Au-"hat" 5 nm.

■ ASSOCIATED CONTENT

Ⓢ Supporting Information

Additional electron microscope images, CD spectra with silica nanoparticles, and UV−vis absorbance data. This material is available free of charge via the Internet at http://pubs.acs.org.

■ AUTHOR INFORMATION

Corresponding Authors

*E-mail: govorov@helios.phy.ohiou.edu.
*E-mail: kotov@umich.edu.

Present Address

[§]989-111 Daedeok-daero, Yuseong-gu, Daejeon, 305-353, Korea.

Notes

The authors declare no competing financial interest.

■ ACKNOWLEDGMENTS

This material is based upon work partially supported by the Center for Solar and Thermal Energy Conversion, an Energy Frontier Research Center funded by the U.S. Department of Energy, Office of Science, Office of Basic Energy Sciences under award number no. DE-SC0000957. We acknowledge support from NSF under grant ECS-0601345; EFRI-BSBA 0938019; CBET 0933384; CBET 0932823; and CBET

1036672. The work is also partially supported by ARO MURI W911NF-12-1-0407 "*Coherent Effects in Hybrid Nanostructures for Lineshape Engineering of Electromagnetic Media*" (N.A.K. and A.G.). The authors thank the University of Michigan's EMAL for its assistance with electron microscopy and for the NSF grant no. DMR-9871177 for funding for the JEOL 2010F analytical electron microscope used in this work. A.O.G. thanks the NSF for support (NSF Project No. CBET-0933415). Use of the computer facilities at the Center for Nanoscale Materials by A.O.G. and Hui Zhang was supported by the U.S. Department of Energy, Office of Science, Office of Basic Energy Sciences, under contract no. DE-AC02-06CH11357.

REFERENCES

(1) Yashima, E.; Maeda, K.; Iida, H.; Furusho, Y.; Nagai, K. *Chem. Rev.* **2009**, *109*, 6102−6211.
(2) Cornelissen, J. J. L. M.; Rowan, A. E.; Nolte, R. J. M.; Sommerdijk, N. A. J. M. *Chem. Rev.* **2001**, *101*, 4039−4070.
(3) Pendry, J. *Science* **2004**, *306*, 1353−1355.
(4) Kildishev, A. V.; Boltasseva, A.; Shalaev, V. M. *Science* **2013**, *339*, 1232009.
(5) Hendry, E.; Carpy, T.; Johnston, J.; Popland, M.; Mikhaylovskiy, R.; Lapthorn, A.; Kelly, S.; Barron, L.; Gadegaard, N.; Kadodwala, M. *Nat. Nanotechnol.* **2010**, *5*, 783−787.
(6) Chen, Y.-H.; Yang, J. T.; Martinez, H. M. *Biochemistry* **1972**, *11*, 4120−4131.
(7) Schaaff, T. G.; Whetten, R. L. *J. Phys. Chem. B* **2000**, *104*, 2630−2641.
(8) Zhou, Y.; Yang, M.; Sun, K.; Tang, Z.; Kotov, N. A. *J. Am. Chem. Soc.* **2010**, *132*, 6006−6013.
(9) Chen, W.; Bian, A.; Agarwal, A.; Liu, L.; Shen, H.; Wang, L.; Xu, C.; Kotov, N. A. *Nano Lett.* **2009**, *9*, 2153−2159.
(10) Mastroianni, A. J.; Claridge, S. A.; Alivisatos, A. P. *J. Am. Chem. Soc.* **2009**, *131*, 8455−8459.
(11) Kuzyk, A.; Schreiber, R.; Fan, Z.; Pardatscher, G.; Roller, E.-M.; Hogele, A.; Simmel, F. C.; Govorov, A. O.; Liedl, T. *Nature* **2012**, *483*, 311−314.
(12) Tang, Y.; Cohen, A. E. *Phys. Rev. Lett.* **2010**, *104*, 163901.
(13) Kuwata-Gonokami, M.; Saito, N.; Ino, Y.; Kauranen, M.; Jefimovs, K.; Vallius, T.; Turunen, J.; Svirko, Y. *Phys. Rev. Lett.* **2005**, *95*, 227401.
(14) Dolamic, I.; Knoppe, S.; Dass, A.; Burgi, T. *Nat. Commun.* **2012**, *3*, 798.
(15) MacLaren, D. A.; Johnston, J.; Duncan, D. A.; Marchetto, H.; Dhesi, S. S.; Gadegaarde, N.; Kadodwala, M. *Phys. Chem. Chem. Phys.* **2009**, *11*, 8413−8416.
(16) Guerrero-Martinez, A.; Auguie, B.; Alonso-Gomez, J.; Dzolic, Z.; Gomez-Grana, S.; Zinic, M.; Cid, M.; Liz-Marzan, L. *Angew. Chem., Int. Ed.* **2011**, *50*, 5499−5503.
(17) Sharma, J.; Chhabra, R.; Cheng, A.; Brownell, J.; Liu, Y.; Yan, H. *Science* **2009**, *323*, 112−116.
(18) Liu, S.; Han, L.; Duan, Y.; Asahina, S.; Terasaki, O.; Cao, Y.; Liu, B.; Ma, L.; Zhang, J.; Che, S. *Nat. Commun.* **2012**, *3*, 1215.
(19) Chen, C.-L.; Zhang, P.; Rosi, N. L. *J. Am. Chem. Soc.* **2008**, *130*, 13555−13557.
(20) Shen, X.; Asenjo-Garcia, A.; Liu, Q.; Jiang, Q.; García de Abajo, F. J.; Liu, N.; Ding, B. *Nano Lett.* **2013**, *13*, 2128−2133.
(21) Auguié, B.; Alonso-Gómez, J. L.; Guerrero-Martínez, A. S.; Liz-Marzán, L. M. *J. Phys. Chem. Lett.* **2011**, *2*, 846−851.
(22) Ma, W.; et al. *Sci. Rep.* **2013**, *3*, 1934.
(23) Hentschel, M.; Schaferling, M.; Weiss, T.; Liu, N.; Giessen, H. *Nano Lett.* **2012**, *12*, 2542−2547.
(24) Gansel, J. K.; Thiel, M.; Rill, M. S.; Decker, M.; Bade, K.; Saile, V.; von Freymann, G.; Linden, S.; Wegener, M. *Science* **2009**, *325*, 1513−1515.
(25) Mark, A. G.; Gibbs, J. G.; Lee, T.-C.; Fischer, P. *Nat. Mater.* **2013**, *12*, 802−807.
(26) Frank, B.; Yin, X.; Schäferling, M.; Zhao, J.; Hein, S. M.; Braun, P. V.; Giessen, H. *ACS Nano* **2013**, *7*, 6321−6329.
(27) Singh, J. H.; Nair, G.; Ghosh, A.; Ghosh, A. *Nanoscale* **2013**, *5*, 7224−7228.
(28) Yan, W.; Xu, L.; Xu, C.; Ma, W.; Kuang, H.; Wang, L.; Kotov, N. A. *J. Am. Chem. Soc.* **2012**, *134*, 15114−15121.
(29) Kawata, S.; Sun, H.-B.; Tanaka, T.; Takada, K. *Nature* **2001**, *412*, 697−698.
(30) Deubel, M.; von Freymann, G.; Wegener, M.; Pereira, S.; Busch, K.; Soukoulis, C. M. *Nat. Mater.* **2004**, *3*, 444−447.
(31) Robbie, K.; Broer, D.; Brett, M. *Nature* **1999**, *399*, 764−766.
(32) Hou, Y.; Li, S.; Su, Y.; Huang, X.; Liu, Y.; Huang, L.; Yu, Y.; Gao, F.; Zhang, Z.; Du, J. *Langmuir* **2013**, *29*, 867−872.
(33) Greene, L.; Law, M.; Goldberger, J.; Kim, F.; Johnson, J.; Zhang, Y.; Saykally, R.; Yang, P. *Angew. Chem., Int. Ed.* **2003**, *42*, 3031−3034.
(34) Fan, Z.; Govorov, A. O. *Nano Lett.* **2010**, *10*, 2580−2587.
(35) Prodan, E.; Radloff, C.; Halas, N.; Nordlander, P. *Science* **2003**, *302*, 419−422.
(36) Shemer, G.; Krichevski, O.; Markovich, G.; Molotsky, T.; Lubitz, I.; Kotlyar, A. B. *J. Am. Chem. Soc.* **2006**, *128*, 11006−11007.
(37) Fan, Z.; Govorov, A. O. *Nano Lett.* **2012**, *12*, 3283−3289.
(38) Mulvaney, P. *Langmuir* **1996**, *12*, 788−800.
(39) Slaughter, L. S.; Wu, Y.; Willingham, B. A.; Nordlander, P.; Link, S. *ACS Nano* **2010**, *4*, 4657−4666.
(40) Yao, H.; Miki, K.; Nishida, N.; Sasaki, A.; Kimura, K. *J. Am. Chem. Soc.* **2005**, *127*, 15536−15543.
(41) Elliott, S. D.; Moloney, M. P.; Gun'ko, Y. K. *Nano Lett.* **2008**, *8*, 2452−2457.
(42) Fan, Z.; Zhang, H.; Govorov, A. O. *J. Phys. Chem. C* **2013**, *117*, 14770−14777.
(43) Maoz, B. M.; van der Weegen, R.; Fan, Z.; Govorov, A. O.; Ellestad, G. A.; Berova, G. N.; Meijer, E. W.; Markovich, G. *J. Am. Chem. Soc.* **2012**, *134*, 17807−17813.
(44) Plum, E.; Fedotov, V. A.; Zheludev, N. I. *J. Opt. A: Pure Appl. Opt.* **2009**, *11*, 074009.
(45) Schwanecke, A. S.; Fedotov, V. A.; Khardikov, V. V.; Prosvirnin, S. L.; Chen, Y.; Zheludev, N. I. *Nano Lett.* **2008**, *8*, 2940−2943.